nature communications



Article

https://doi.org/10.1038/s41467-025-64449-0

Global loss of mountain vegetated landscapes and its impact on biodiversity conservation

Received: 26 February 2025

Accepted: 15 September 2025

Published online: 09 October 2025



Check for updates

Chao Yang ^{1,2}, Haiying Xu^{1,2}, Qingquan Li ^{1,2,3} ✓, Xuqing Wang ⁴, Bohui Tang ⁵, Junyi Chen 6, Wei Tu 12, Yinghui Zhang 1,2, Tiezhu Shi 1,2, Min Chen 6,7,8, Wei Ma⁹. Huizeng Liu © 10,11 & Jonathan M. Chase © 12,13

Accelerating human encroachment and natural disasters are causing substantial loss of mountain vegetated landscapes, threatening biodiversity conservation and ecosystem sustainability. The global-scale quantification of the magnitude, variability and drivers of the loss of mountain vegetated landscapes, and its impact on biodiversity conservation, however, has been lacking. Here, we combine global datasets on mountain boundaries, land use, natural disasters, and protected and biodiversity hotspots together with largescale earth observation data to quantify global mountain vegetated landscape loss, as well as its variation and potential drivers from 2000 to 2020. Overall, we find widespread but uneven mountain vegetated landscape loss across the globe, of which ~89% can be attributed to human expansion, primarily agriculture, with small contributions of human settlement growth and mining. About ~11% of mountain vegetated landscape loss can be attributed to natural disasters, primarily through drought. We also observe that ~56% of global mountain vegetated landscape loss occurred within protected areas and in areas with high richness of threatened mountain-occurring species, indicating the urgency of improving protection in these areas of loss. Our results can help formulate conservation strategies and contribute to sustainable development.

Mountain ecosystems play a disproportionate role in contributing to global biodiversity, carbon dynamics, water supply and climate stability¹⁻⁴. At the same time, geographically and biologically diverse mountain ecosystems tend to be ecologically fragile⁵. Vegetated landscapes within these mountains, including forests, shrublands and grasslands, influence the health and sustainability of the entire mountain ecosystem⁵⁻⁸ by preventing soil and water loss, providing shelter and food for wildlife and supporting the development of local

¹MNR Key Laboratory for Geo-Environmental Monitoring of Great Bay Area & Guangdong Key Laboratory of Urban Informatics & Shenzhen Key Laboratory of Spatial Smart Sensing and Services, Shenzhen University, Shenzhen, China. 2School of Architecture and Urban Planning, Shenzhen University, Shenzhen, China. 3Guangdong Laboratory of Artificial Intelligence and Digital Economy (SZ), Shenzhen, China. 4Center for Hydrogeology and Environmental Geology, China Geological Survey, Baoding, China. 5 Faculty of Land Resource Engineering, Kunming University of Science and Technology, Kunming, China. ⁶Key Laboratory of Virtual Geographic Environment (Ministry of Education of PRC), Nanjing Normal University, Nanjing, China. ⁷Jiangsu Center for Collaborative Innovation in Geographical Information Resource Development and Application, Nanjing, China. 8International Research Center of Big Data for Sustainable Development Goals, Beijing, China. 9School of Civil Engineering, Chongqing Jiaotong University, Chongqing, China. 10Institute for Advanced Study & Shenzhen University, Shenzhen, China. 11 Tiandu-Shenzhen University Deep Space Joint Laboratory, Shenzhen University, Shenzhen, China. 12 German Centre for Integrative Biodiversity Research (iDiv) Halle-Jena-Leipzig, Leipzig, Germany. 13 Department of Computer Science, Martin Luther University Halle-Wittenberg, Halle (Saale), Germany. e-mail: ligg@szu.edu.cn

economies (e.g., providing wood, medicinal herbs and food for local residents)⁹⁻¹¹. As a result, sustainably managing mountain ecosystems is one of the targets of the 2030 Agenda for Sustainable Development of the United Nations (SDG 15.4)¹².

Despite their disproportionate role in supporting biodiversity and ecosystem services, mountain ecosystems continue to be widely developed and degraded^{13,14}, including hillside urbanisation^{15–18}, agriculture expansion^{19–21} and mining^{22,23}. Although these developments bring economic benefits, they simultaneously lead to the loss of vegetated landscapes within these mountains^{24–26}. At the same time, anthropogenic climate change is increasing the frequency and intensity of natural disasters, including wildfires, floods, landslides and droughts^{27–31}, which can alter vegetation within these landscapes^{32–36}.

Mountain vegetation landscapes (MVL) are being lost across the world due to both human expansions and natural disasters, which can bring serious consequences to biodiversity conservation and sustainable development goals. In 2022, the Convention on Biological Diversity adopted the Kunming-Montreal Global Biodiversity Framework as an urgent response to biodiversity loss³⁷, which will require accurate information of global MVL loss to promote the targets of this framework. Unfortunately, the magnitude of MVL loss and its distribution across the world, as well as the contribution of different sources to this loss (e.g., different kinds of human expansions, natural disasters), are largely incomplete. Such information would provide essential guidance for understanding and potentially mitigating these changes.

Here, we present a global assessment of the magnitude and distribution of MVL loss at 30 m resolution in response to both human expansions and natural disasters from 2000 to 2020 using global datasets on mountain boundaries, human land use, and natural disasters together with Landsat imagery. In particular, we use a Landsat imagery-derived vegetation index to quantify vegetation reduction associated with natural disasters (see details in "Methods"). We estimate MVL loss from changes in human land use, including (i) human settlement growth, (ii) agriculture expansion, and (iii) mining. We estimate MVL loss from natural disasters (a net loss after deducting restored and recovering areas), including (vi) wildfires, (v) floods, (vi) landslides, and (xii) droughts ("Methods"). We separately consider MVL loss across ten global mountain regions. We also consider how MVL loss is aligned with current biodiversity conservation priorities by examining loss within protected areas (PAs) (using the World Database of Protected Areas [WDPA]) and from areas with high richness of threatened mountain-occurring species (AHRTMS) (using the IUCN Red List of threatened species) (Methods). Finally, we validate our results using more than 16,400 high-resolution (≤5 m) random samples to confirm the accuracy of MVL loss (see last part of Methods). We find an overall accuracy of ~88.2% of the global mapping, with a high producer's accuracy (90.7%) and user's accuracy (84.0%) of MVL loss (Supplementary Table 1).

Results

Widespread loss of global MVL

Overall, we found widespread global MVL loss of ~ 356,549.9 km² from 2000–2020, accounting for ~1.9% of the total initial MVL area, as a result of both human expansion and natural disasters (Fig. 1a and Supplementary Table 2). However, only ~11% of this loss could be attributed to natural disasters, primarily drought, with the remaining 89% of the loss of MVL attributed to human expansion over the 20-year observation period. This human-mediated loss of MVL was mainly due to agriculture expansion (contributing ~83%), with considerably less due to human settlement growth (~5%) and mining (~1%) (Fig. 1a).

Of the total observed MVL loss, 57% was in forests, 25% from grasslands, and 18% from shrublands (Fig. 1b). Across these vegetation types, human expansions (i–iii) collectively accounted for over 81% of the MVL loss (Fig. 1c). Among all drivers, agriculture expansion was the

primary driver of forest, shrubland, and grassland loss, followed by drought and then human settlement growth (Fig. 1c and Supplementary Table 2).

Spatial unevenness of MVL loss across regions

The global distribution of MVL loss was highly uneven across regions (Table 1). More than 90% of global MVL losses were concentrated among seven regions: East Asia (16.0%), North America (15.6%), Middle East (14.0%), Europe & Russia (13.3%), Sub-Saharan Africa (11.5%), Latin America (11.0%) and Southeast Asia (10.5%) (Table 1). By contrast, Central and South Asia, as well as Oceania, account for only 8.1% of the total global loss (Table 1). However, when we estimated relative loss (% of their initial MVL area), rather than absolute loss, we found lower relative losses in East Asia, Latin America, Europe & Russia and North America (~1.3–1.7%) owing to their large initial MVL area, and higher relative loss in Middle East (6.2%), Sub-Saharan Africa (3.2%) and Central Asia (3.0%), which had a lower initial MVL area (Table 1). This indicates that mountains in these regions are under disproportionate pressure and are in urgent need for protection and restoration.

Most of the MVL loss in the Middle East and Central Asia was from grasslands, while losses in other regions were mostly from forest losses (Supplementary Fig. 3). Notably, North America experienced the greatest loss of forests, and the Middle East experienced the greatest losses of shrublands and grasslands (Table 1). Forest losses from Southeast and East Asia and Europe & Russia (14.3–16.1%), shrubland losses from Latin America, Europe & Russia and North America (14.2–16.7%), and grassland losses from East Asia (24.2%) were also substantial (Table 1). While such forest losses have been documented (19,20,24,25,38), losses of grassland and shrubland have not been fully documented on a global scale.

Human expansion was the largest contributor to MVL loss across all regions (ranging from 77.3% to 99.1%; Supplementary Table 3), primarily due to agriculture (more than 69% in all regions) (Fig. 2a). However, there was regional variation in the intensity of MVL loss due to other drivers. For example, human settlement growth was most intense in Latin America, as well as South and East Asia, owing primarily to widespread mountain urbanisation projects in these regions^{15–17,39}. In East Asia, and Europe & Russia, MVL loss due to mining was more intense, likely because of high mineral export²³. Drought ranked as the second largest contributor to MVL loss across nine of the ten world regions, with Sub-Saharan Africa being the only exception. (Fig. 2a and Supplementary Table 3). For forest loss, the drivers were similar to the overall MVL loss (Fig. 2b). However, drought contributed disproportionately to shrubland loss in North America (48.9%) and Latin America (41.3%) compared to other regions (Fig. 2c), while human settlement growth contributed disproportionately to grassland loss in Latin America (13.6%) and East Asia (10.9%) compared to other regions (Fig. 2d).

Spatial coincidence of MVL loss and conservation priorities

We examined how MVL loss over the 20-year observation period aligned with current biodiversity conservation priorities by quantifying MVL loss within protected areas (PAs) and areas with high richness of threatened mountain-occurring species (AHRTMS) (Supplementary Figs. 4 and 5). In all, there were $\sim 45,011.6~\rm km^2$ of MVL loss within PAs (accounting for 1.3% of the initial MVL area of PAs) and $\sim 169,289.9~\rm km^2$ MVL loss within AHRTMS (accounting for 2.4% of the initial MVL area of AHRTMS) (Supplementary Table 4). After excluding AHRTMS located within PAs, we observed that 55.7% of the total global MVL loss occurred within PAs (12.6%) and in AHRTMS-outside of PAs (43.1%) (Fig. 3a). This emphasises that even since the year 2000, a substantial amount of these mountain habitats that are protected and/or of particular importance for threatened species have lost their natural vegetation, primarily via human activities such as agriculture expansion (Fig. 3b). In fact, nearly three-fifths of the MVL loss within PAs

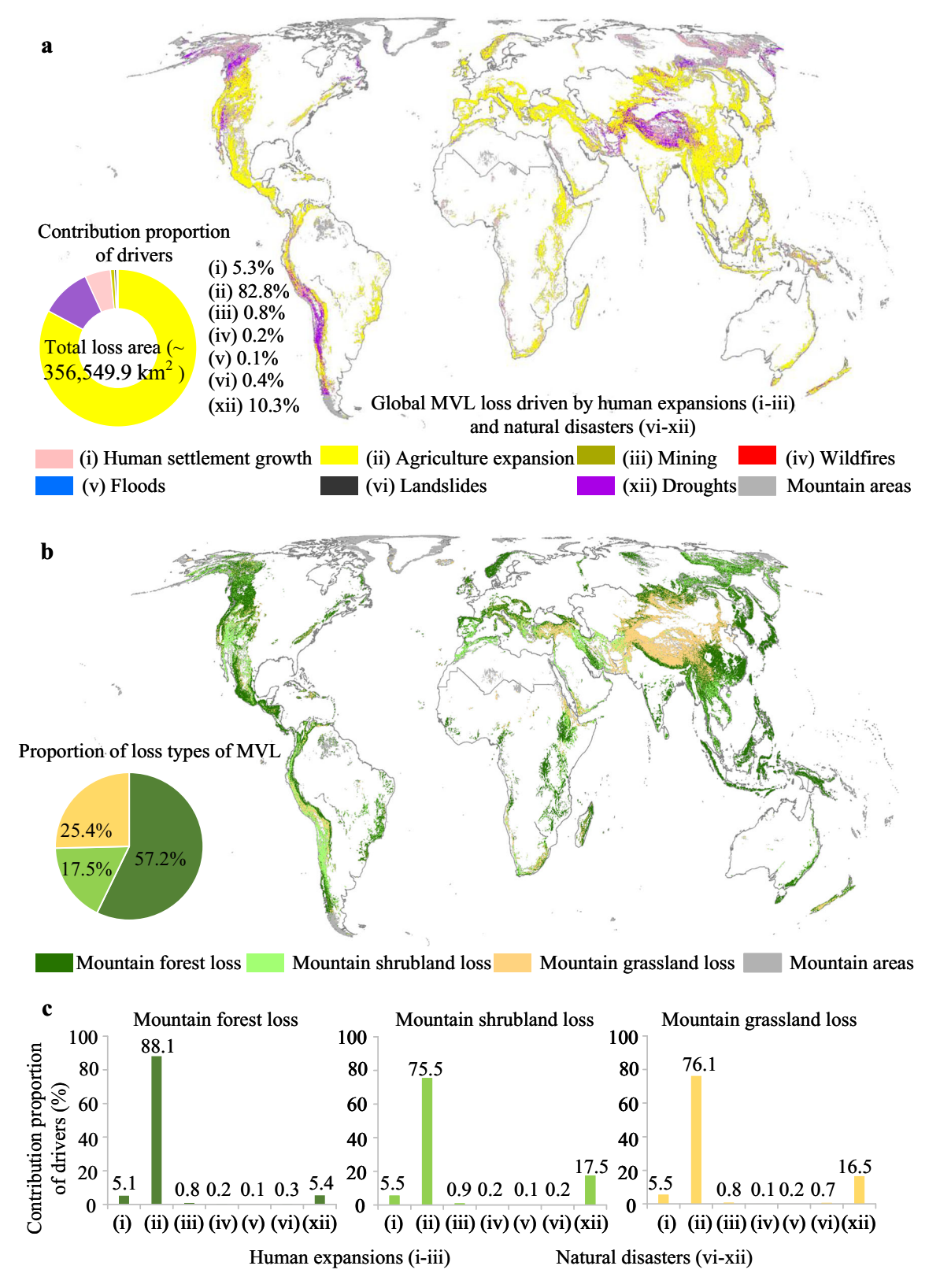


Fig. 1 | **Global MVL loss for the period 2000 to 2020.** a Spatial pattern of global MVL loss at 30-m resolution. The map reports seven drivers caused MVL loss, including (i) human settlement growth, (ii) agriculture expansion, (iii) mining, (iv) wildfires, (v) floods, (vi) landslides and (xii) droughts. b Loss types and proportions of global MVL loss. The map includes three loss types (forest, shrubland and

grassland.) and their proportions (% of total global MVL loss). ${\bf c}$ The contribution proportion of drivers to global MVL loss types. The map includes loss drivers of forest, shrubland and grassland. The background map (global mountain areas) was defined by GMBA (v2.0 standard, https://www.earthenv.org/mountains) (see Supplementary Fig. 1).

Table 1 | The distribution of global MVL loss across ten regions from 2000 to 2020

Regions	MVL loss (% of total global MVL loss from 2000–2020)	Sub-MVL loss (% of loss of the global total of that vegetation type from 2000 to 2020)			Initial MVL area in 2000 (10 ⁵ km ²)	Relative MVL loss (% of their initial
		Mountain for- est loss	Mountain shrub- land loss	Mountain grass- land loss		MVL area)
Sub-Saharan Africa	11.5%	11.1%	9.2%	14.0%	12.7	3.2%
Southeast Asia	10.5%	14.9%	10.7%	0.5%	16.7	2.2%
Middle East	14.0%	5.2%	24.0%	26.9%	8.1	6.2%
South Asia	3.6%	2.9%	1.9%	6.5%	8.0	1.6%
Central Asia	2.6%	1.5%	1.0%	5.9%	3.0	3.0%
East Asia	16.0%	16.1%	3.7%	24.2%	37.9	1.5%
North America	15.6%	19.2%	16.7%	7.0%	33.6	1.7%
Latin America	11.0%	12.8%	14.2%	4.7%	24.5	1.6%
Europe & Russia	13.3%	14.3%	16.3%	9.1%	37.2	1.3%
Oceania	1.9%	2.0%	2.3%	1.3%	5.1	1.3%

It includes the MVL loss and sub-MVL loss from forest, shrubland and grassland. MVL/sub-MVL loss (% of total loss from 2000-2020) indicates the proportion of MVL/sub-MVL loss in each region. Relative MVL (% of their initial MVL area) represents the proportion of MVL loss in each region to their initial MVL area (MVL loss area/initial MVL area in 2000).

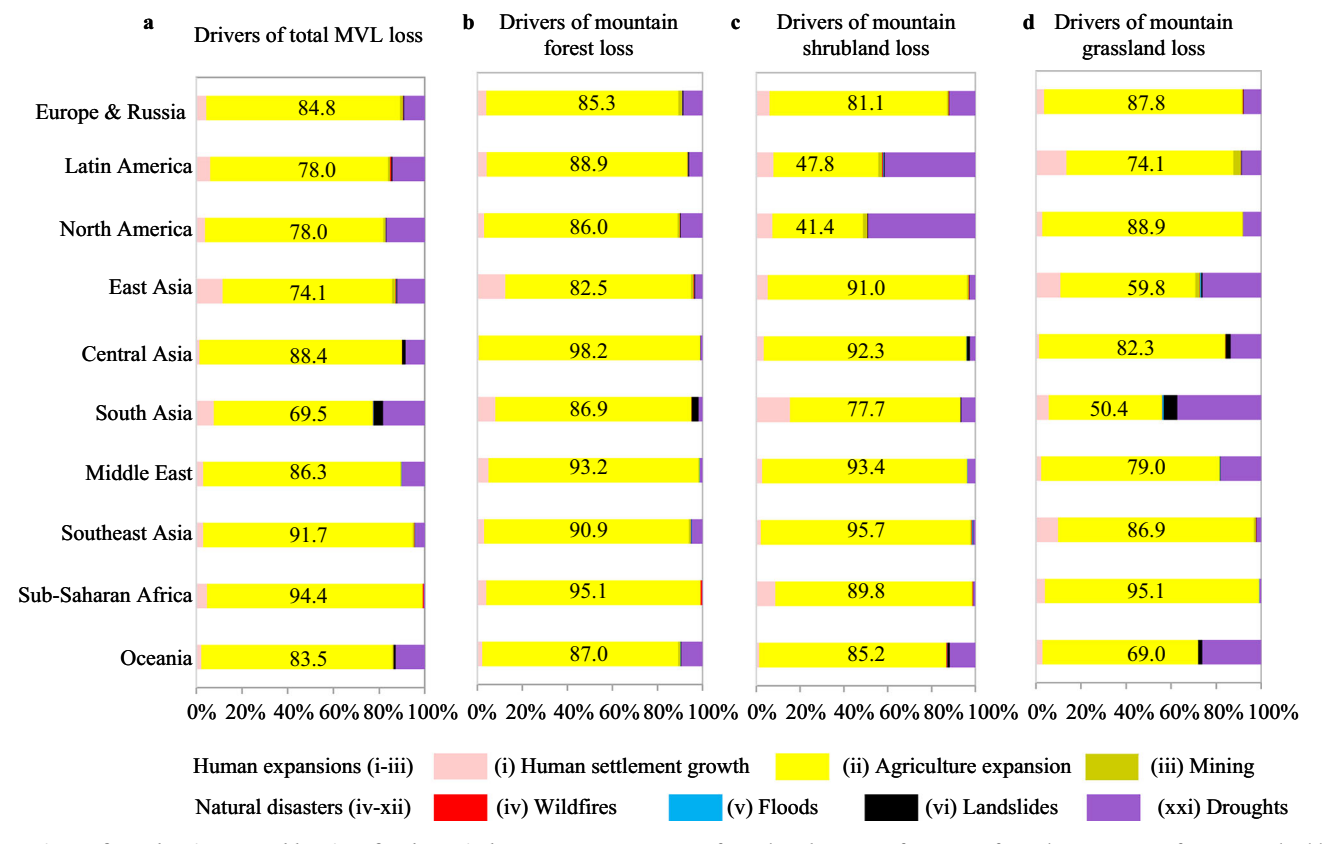


Fig. 2 | Drivers of MVL loss in ten world regions for the period 2000 to 2020. a Drivers of MVL loss. b Drivers of mountain forest loss. c Drivers of mountain shrubland loss. d Drivers of mountain grassland loss.

(7.9% of total global MVL loss) occurred after the PAs were officially designated (established before 2000) (Fig. 3a), with almost 77% of this as a result of human expansions, rather than natural disasters. This suggests that the legal effect of mountain PAs has not been fully realised in many parts of the world.

AHRTMS located outside of PAs are not legally protected, but contain high concentrations of mountain-occurring threatened species (Supplementary Fig. 4). As a result, MVL loss within these areas poses a large challenge to biodiversity conservation. We observed that MVL loss within AHRTMS-outside of PAs is mainly concentrated in

Southeast Asia, southern East Asia and eastern Sub-Saharan Africa (Supplementary Fig. 5), where attaining protected status would be particularly urgent. Prioritising the increase of PAs in these areas could allow a better response to the United Nations agreement of globally expanding PAs to slow or reverse biodiversity declines^{40,41}.

Discussion

Overall, we find widespread, but geographically variable MVL loss since the year 2000, much of which can be attributed to human activities and in particular, agricultural and human settlement

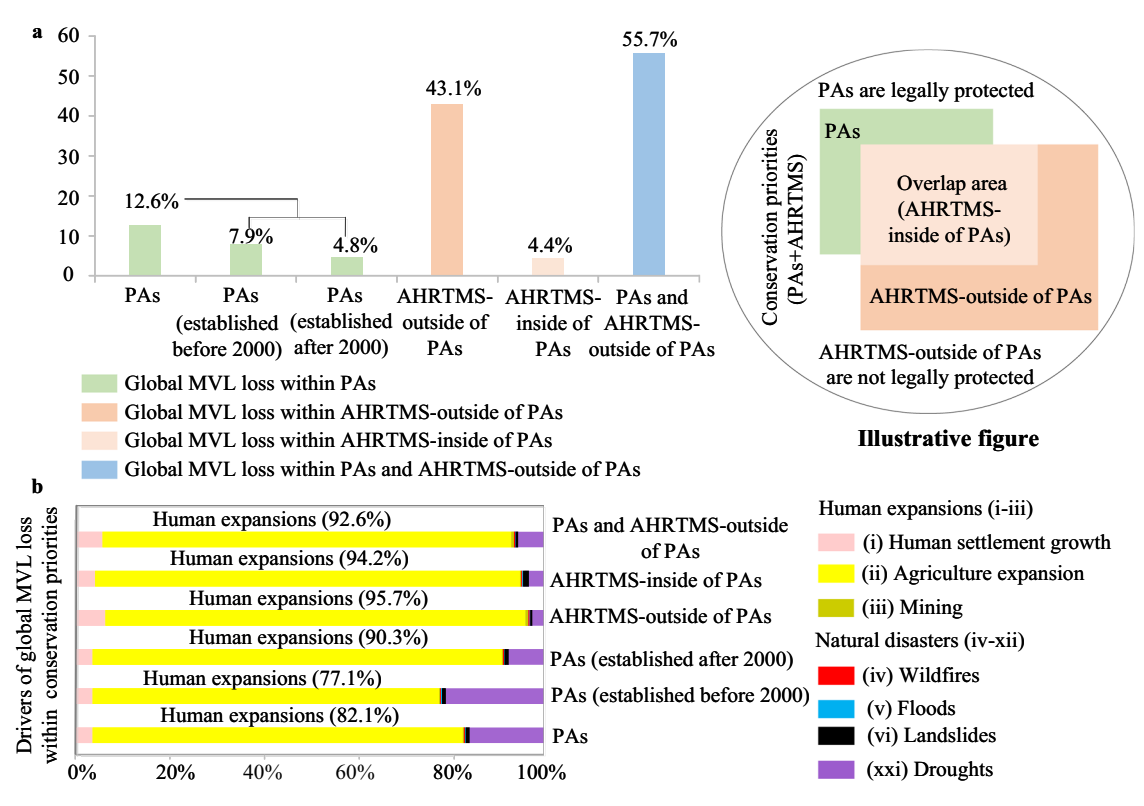


Fig. 3 | Global MVL loss in areas of biodiversity conservation priorities (i.e., PAs (protected areas) and AHRTMS (areas with high richness of threatened mountain-occurring species)) for the period 2000–2020. a The proportions of

MVL loss within PAs and AHRTMS (% of total global MVL loss). **b** Drivers of MVL loss within PAs and AHRTMS.

expansion (Fig. 1a). Indeed, approximately 88% of the extent of expansion of agriculture and human settlement into mountains (total expansion area reaching - 374,175.8 km²) has led to MVL loss in the past two decades (Supplementary Fig. 6 and Supplementary Table 2). This encroachment into MVL may be related to the high economic values of vegetated land (e.g., harvesting) and soil quality for crop growth, in addition to the landscape value for human settlement projects 15,16,24,42. Furthermore, the MVL loss driven by the growth of human settlement has led to an increase in wildland–urban interfaces (i.e., the concentration areas of human-environmental conflicts and risks) 43, which may increase risk to humans due to wildfires, as well as the spread of zoonotic diseases 44,45. More importantly, these lost areas of MVL have been converted to human settlements, which may increase the risk of human-wildlife conflicts 46-49.

Although mountain mining only contributes ~ 1% to the loss of global MVL (Fig. 1a), it has resulted in 31,432 mining patches (per patch area > 1 ha) in mountain areas, 37.4% of which are located within PAs (1094 patches) and AHRTMS-outside of PAs (10,672 patches) (Supplementary Fig. 7). Mine tailings (the residue remaining after mineral processing) and infrastructures related to mining sites can seriously threaten natural environments (e.g., polluting downstream water resources) and their biodiversity^{50,51}. Furthermore, human populations are increasingly dependent on water resources from mountainous areas⁵², and thus development of mines and their tailings can pose a large threat of pollution to water supplies^{53,54}.

While there were substantial losses of MVL due to human expansions, about 11% of the loss can be attributed to natural disasters, mostly due to drought (Fig. 1a). Indeed, the recent increase in drought severity worldwide has led to typically dry areas becoming drier, and more humid regions also experiencing a drying trend⁵⁵. The MVL loss caused by natural disasters was less than that driven by human expansions, which may be attributed to the natural recovery of vegetation over time in damaged areas or the transformation between

vegetation types (e.g., forest converted to shrubland or grassland)⁵⁶⁻⁶¹. In addition, the occurrence of different natural disasters can directly or indirectly accelerate the extinction risk of endangered species⁶²⁻⁶⁵. For example, wildfires and landslides can immediately kill species, while droughts can lead to water and food shortages, which is particularly problematic when these disasters occur within PAs or AHRTMS.

Mountain PAs and AHRTMS can play important roles in conserving mountain biodiversity when human intrusion is minimised⁶⁶⁻⁶⁸. However, we found that ~ 55.7% of global MVL loss is still located within these areas, comprising 12.6% within PAs and 43.0% in AHRTMS outside of PAs. This was primarily as a result of human land use increasing the human-threatened species conflict risks and diminishing a number of important ecosystem functions and services (e.g., landscape connectivity, habitat quality and carbon storage)⁶⁹⁻⁷³. Therefore, it is crucial to strengthen legal enforcement in existing PAs (e.g., through community co-management, "sky-ground" monitoring systems, judicially enforced protection orders and transboundary governance)^{74,75}. Furthermore, given the high biodiversity and concentration of threatened species within AHRTMS, incorporating high-risk AHRTMS outside of PAs into formal PA networks may help to mitigate biodiversity loss in these vulnerable regions. Likewise, exploring land sparing (i.e., separating land for conservation from land for crops)^{68,76} or fragmented land replacement (i.e., replacing fragmented cropland in mountains with fragmented vegetated land in plains, Supplementary Fig. 8) in areas under agriculture expansion in mountains could achieve a win-win scenario for development and mountain conservation. We also call on the governments in areas with high amounts of MVL loss to strengthen economic transformation and regulate human activities to prevent the further expansion of MVL loss.

In summary, our fine-scale map of global MVL loss identifies the spatial distribution of MVL loss (including seven potential drivers). The accuracy of our global MVL loss map was consistently high and above acceptable levels (Supplementary Table 1). Moreover, our global MVL

loss map also provides timely, transparent and critical insights for sustainable development and biodiversity conservation, which can help researchers, governments and regulatory agencies to make targeted protection and recovery strategies. For example, the relative contributions of human expansions and natural disasters to global MVL loss can help to provide more accurate parameters for improving climate change scenario modelling⁷⁷. The spatial pattern of MVL loss (especially for 30 m resolution of MVL loss within PAs and AHRTMS) can identify severe loss areas at national or local scales, which can assist their governments to achieve ecological and biodiversity conservation aligned with the Kunming Montreal Global Biodiversity Framework (e.g., establishing new protected areas in severe loss areas). By characterising global erosion of MVL and its driver attribution, we hope our study will inform and support conservation efforts aimed at preserving mountain vegetated ecosystems for future generations.

Methods

Mapping global mountain vegetated landscapes

We first mapped MVL in 2000 as a base map from which to estimate changes. To do so, we combined a global land-cover dataset in 2000 with a global mountain dataset. For land cover, some moderate spatial resolution products exist, such as the MODIS Land Cover Type from 2001 to 2016 (500 m), the ESA Climate Change Initiative (ESA-CCI) from 1992 to 2015 (300 m), Copernicus Global Land Cover Lavers (CGLS-LC100) from 2015 to 2019 (100 m), Finer Resolution Observation and Monitoring of Global Land Cover product (FROM-GLC) in 2010, 2015 and 2017 (30 m/10 m), Globeland30 in 2000, 2010 and 2020 (30 m), global 30 m land cover classification with a fine classification system (GLC FCS30D) in 2000 and 2020 (30 m) and ESA's WorldCover in 2020 and 2021 (10 m)⁷⁸⁻⁸¹. However, we chose GLC FCS30D in our study mainly due to its high spatial resolution, suitable temporal resolution, fine classification system and more stable accuracy on a global scale compared to other 30-m global land-cover products⁸². The GLC FCS30D product was produced by combining time series of Landsat imageries and high-quality training data from the Global Spatial Temporal Spectra Library on the Google Earth Engine cloud computing platform and presented at an approximately 30-m resolution⁸⁰. The accuracy of GLC FCS30D has been validated using numerous validation samples, with an overall accuracy of more than 81 %83,84 (available from Zenodo: https://doi.org/10.5281/zenodo. 8239305), and it has been extensively used for a variety of applications^{45,85}. For mountain delineation, commonly used global datasets include the United Nations Environment Programme-World Conservation Monitoring Centre (UNEP-WCMC) mountain inventory86 and the Global Mountain Biodiversity Assessment (GMBA)87,88 inventories (both standard and broad versions). After checking these mountain datasets, we found that the UNEP-WCMC dataset omits important mountain areas (e.g., southeastern Russia, central New Zealand, northern Norway) and overestimates some mountainous areas (e.g., northwestern China) (Supplementary Table 5). Likewise, the broad GMBA version incorporates not only mountainous terrain but also extends into adjacent landscapes⁸⁸(Supplementary Table 5). On the other hand, the standard GMBA version (v2.0 standard) (https://www.earthenv.org/mountains) was better suited and addressed the aforementioned issues, which we thus chose in our study. This dataset delineates mountains covering ~ 18.2% of the Earth's land surface (Supplementary Fig. 1).

To combine these datasets, we first converted the mountain boundary polygons into a grid image of 30 m resolution using the polygon to raster tool of ArcGIS. We then reclassified the GLC_FCS30D product into six land cover types following Zhang et al.⁸⁰: cropland, impervious surface, forest, grassland, shrubland and other land. In this dataset, cropland is defined as land used for crop cultivation, including rain-fed croplands, herbaceous cover, and tree/shrub-covered croplands (e.g., orchards, plantations)⁸⁰; impervious surface refers to

hardened surfaces composed of artificial materials, including constructed materials (e.g., cement, asphalt and bricks) and artificially compacted surfaces (e.g., paved grounds, rocks and building foundations)80; forest, shrubland, and grassland are defined as land cover types dominated by trees, shrubs, and herbaceous plants, respectively. Forests include various types (e.g., evergreen broadleaved forest, deciduous broadleaved forest, and mixed-leaf forest); shrublands include both evergreen and deciduous types⁸⁰. Following ecological principles, vegetation structure, the Intergovernmental Panel on Climate Change guidelines, and the Food and Agriculture Organisation Global Ecological Zones, these three classes represent the primary vegetated land cover types in global mountain ecosystems⁸⁹⁻⁹¹. Therefore, we selected forest, shrubland, and grassland to define different vegetated landscapes, with all other classes designated as non-vegetated landscapes. We calculated mountain vegetated landscapes (MVL) by calculating spatial overlays between these vegetated landscapes with standardised mountain boundaries (GMBA v2.0), and defining all overlapping pixels as MVL. All calculations involving the map area were performed in WGS 84/Equal Earth Greenwich projection. Overall, we found a total area of approximation 18,681,548.8 km² of MVL in 2000 (Supplementary Table 6).

Tracking global MVL loss

(1) Human expansions-driven MVL loss. To track MVL loss since 2000 due to the expansion of human activities, we collected multi-source thematic datasets that quantify possible human activities in mountain areas. These included the impervious surface dataset (30 m resolution) and cropland dataset (30 m resolution) from 2000 and 2020, both of which are subsets of the GLC FCS30D, as well as global mining distribution data (polygons). For global mining distribution data, we combined two recent global mining datasets from Maus et al.²² (total 44,929 polygons, covering 101,583 km²) and Tang et al.²³ (total 74,548 polygons, covering 66,000 km²). These two datasets provide spatially explicit estimates of the area directly used for surface mining on a global scale (including large-scale and artisanal and small-scale mining), and the polygons cover all ground features related to mining activities (e.g., open cuts, tailing dams, waste rock dumps, water ponds, processing infrastructure). They were produced using remote sensing analysis of high-resolution, publicly available satellite imagery in recent years (e.g., around 2020; images with ≤10 m resolution in Google Earth and Sentinel-2) (details in refs. 22,23). The overall accuracies of these two global mining datasets calculated from the validation points were 88.3% (for Maus et al.²²) (version 2, https:// doi.org/10.1594/PANGAEA.942325) and ~ 92% (for Tang et al.²³) (version 2, https://zenodo.org/records/7894216).

We merged the two global mining datasets to compensate for the potential omission of global mining areas from the different datasets using union analysis in ArcGIS 10.8. After merging, a combined global mining dataset was obtained (i.e., 81,962 polygons, covering 120,413 km²) (Supplementary Fig. 9). We then converted all polygons into a grid image of 30 m resolution using the polygon to raster tool of ArcGIS. To avoid overestimation of MVL loss caused by pixel overlap between datasets, we used spatial overlay analysis to detect overlapping pixels of impervious surface, cropland and mining areas. If there are overlapping pixels, we assigned their attributes to mining areas, because the mining data holds better spatial resolution and accuracy.

We quantified global MVL loss driven by human expansion according to the following rules:

(i) Human settlement growth. We used the expansion of impervious surface to reflect the growth of human settlements ^{92,93}. To do so, we used a pixel-level change detection method to identify the pixels that were impervious surface in 2020, but not in 2000. The MVL loss driven by human settlements denotes the pixels of MVL in 2000 that were transformed into human settlements by 2020 (Fig. 1a).

(ii) Agriculture expansion. We used the expansion of cropland to reflect increases in agriculture. To do so, we also used the change detection method to identify pixels that were defined as cropland pixels in 2020 but not in 2000. The MVL loss driven by agriculture expansion denotes the pixels of MVL in 2000 that were transformed into agriculture by 2020 (Fig. 1a).

(iii) Mining. We used spatial overlay analysis to detect the intersection pixels between mining areas and MVL. The MVL loss driven by mining denotes that the pixels of MVL in 2000 that were transformed into mining surface by 2020 (Fig. 1a).

(2) Natural disasters-driven MVL loss. To track MVL loss due to natural disasters, including wildfires, floods, landslides and drought, we collected multi-source natural disasters datasets that occurred during 2000-2020. For wildfires, we used global annual burned area maps (GABAM) (30-m resolution) (available from https://doi.org/10.7910/ DVN/3CTMKP), which were generated via an automated pipeline based on Google Earth Engine using all the available Landsat images (details in ref. 94), and define the spatial extent of wildfires that occur in a given year, but not previous years. We selected GABAM because it covers the appropriate time period and has low commission and omission errors, with high spatial resolution (30 m)94. We collected global flood data (2000-2018) from the Global Flood Database (GFD) (http://globalflood-database.cloudtostreet.info/), it was developed based on flood events reported by the Dartmouth Flood Observatory and 250 m resolution Terra and Aqua MODIS images95. We obtained global landslides data (13,437 points from 2001 to 2020) from the NASA Global Landslide Catalogue (NASA-GLC) (https://catalog.data.gov/dataset/ global-landslide-catalog-export), which was developed with the goal of identifying rainfall-triggered landslide events, regardless of size, impacts or location 96,97. We converted landslides to polygons using buffer analysis according to their records in GLC (from small to large, attributes 1-5%). We set buffer distances to 1 km (small event), 5 km (medium event), 10 km (medium to large event including multiple sliding events over a region), 15 km (large to massive event including many landslides), 20 km (massive event or multiple large events), then all landside polygons were converted into a raster image with 30 m resolution using ArcGIS 10.8. For drought, we obtained global data on the temperature-vegetation dryness index (TVDI) with 1 km resolution (2000–2020) data from the National Earth System Science Data Centre of China (http://www.geodata.cn/). TVDI was produced using 1km MODIS land surface temperature (i.e., MOD11A2) together with vegetation index products (i.e., MOD13A2) based on the Google Earth Engine platform⁹⁸. We divided quantitative drought values based on give ranges of TVDI from 0 to 1 at intervals of 0.2 (i.e., extremely wet, wet, moderate, dry, and extremely dry)⁹⁹. We defined areas with drought as those with dry and extremely dry conditions (i.e., 0.6 < TVDI ≤ 1.0), where the probability of vegetation mortality was highest 99,100.

For areas affected by floods and drought, we resampled data to 30 m resolution using the nearest neighbour sampling to match other data. To avoid overestimated MVL loss caused by pixel overlap between datasets, we used spatial overlay analysis to detect overlapping pixels from areas burned, flooded, exposed to landslides or experiencing droughts. If there were overlapping pixels, we assigned overlapping pixels according to the priority of original spatial resolution (i.e., landslides > burned areas > floods > drought). If there were overlapping pixels between human expansion and natural disaster-driven MVL loss, we assigned overlapping pixels to the former.

Because some MVL can remain intact (or recovered) after long-term natural disasters, we used a strict Normalised Difference Vegetation Index (NDVI) threshold to obtain a net loss of MVL. NDVI, defined as the relationship operation between near-infrared (NIR) and red (R) bands of satellite imagery (i.e., NDVI = (NIR - R)/(NIR + R)), varies between -1 and 1, where higher values closer to 1 indicate dense

vegetation coverage, while values closer to 0 suggest very little vegetation, and values less than 0 indicate no vegetation^{101,102}. We collected all available global Landsat images (TM/ETM+/OLI, 30-m resolution) in 1999 (the year prior to our focus) and 2021(the year after our focus) from the United States Geological Survey (USGS) (https://www.usgs.gov/), and used the Google Earth Engine platform and maximum value composites method to generate annual composite NDVI data (before and after our study period).To eliminate spectral response discrepancies among sensors (TM/ETM+/OLI), we applied relative radiometric normalisation to the TM, ETM+ and OLI imagery using the cross-sensor transformation coefficients proposed by Roy et al.¹⁰³, ensuring the spatiotemporal consistency of NDVI.

We quantified MVL losses driven by four natural disasters: wild-fires, floods, landslides, and droughts. To do so, we used a consistent spatial overlay and NDVI thresholding approach. We first delineated MVL in 2000 and intersected them with respective disaster footprints (burned/flooded/landslide/drought areas). If the NDVI at the end of the study period in a given pixel is less than or equal to 0.1, while it was greater than 0.1 at the start of the period, these pixels are labelled as MVL loss^{104,105}(Fig. 1a).

The MVL loss in separate ten world regions

To examine the spatial pattern of MVL in different geographical zones, we divided the world into ten separate regions by merging national administrative boundaries (i.e, Sub-Saharan Africa, Southeast Asia, Middle East, South Asia, Central Asia, East Asia, North America, Latin America, Europe & Russia, and Oceania) (Supplementary Fig. 2). We then quantified the MVL loss (including total MVL loss and MVL loss types, Fig. 2) and the contribution of drivers (Fig. 2) in these ten regions through spatial analysis (zonal statistics tool of ArcGIS) between global MVL loss layer and the regions (Supplementary Table 2).

The MVL loss within PAs and AHRTMS

To quantify MVL loss within protected areas (PAs) and areas with high richness of threatened mountain-occurring species (AHRTMS), we first mapped mountain PAs and AHRTMS using global PA distributions and the IUCN Red List of threatened species. We collected the global distribution of PAs from the WDPA (version 2023.11, https://www.protectedplanet.net/en) provided by the United Nations Environment Programme's World Conservation Monitoring Centre. PAs are stratified into pre-2000 and post-2000 cohorts based on establishment year attributes within the geodatabase. We overlapped the distribution of mountains with PA designations to identify the mountain PAs. After excluding the point features and merging overlapped features, we obtained 52,144 global mountain PAs (a total of 57,363 polygon features), comprising an area of approximately 4,799,535.1 km² (Supplementary Fig. 4a).

The AHRTMS were designated as important biodiversity habitats based on the number of mountain-occurring threatened species (mammals, amphibians, reptiles, birds and plants) they contain. Our AHRTMS was not completely consistent with the global database of IUCN's key biodiversity areas¹⁰⁶ because we only focus on mountain areas that represent areas of the highest richness of threatened mountain-occurring species. To identify AHRTMS, we used the IUCN Red List of threatened species, including distribution information of mammal, amphibian, reptile and plant species (version 6.3, https:// www.iucnredlist.org, updated on December 2022), and for birds, the Birdlife International website (version 2022.02, http://datazone.birdlife. org/home). The Red List classifies threatened species as critically endangered (CR), endangered (EN), and vulnerable (VU). We extracted all threatened species (CR + EN + VU) that occurred in mountains, giving a total number of 12,562 species, including mammals (n = 2019), amphibians (n = 2991), reptiles (n = 1576), birds (n = 2140) and plants (n = 3836). We weighted threatened categories according to ref. 107 (i.e., CR is categorised as 3, EN is categorised as 2, and VU is categorised

as 1). We then generated $1 \times 1 \, \text{km}^2$ grid cells with mountain boundaries, and identified the weighted threatened species in every grid to produce a map of threatened species richness. We normalised the threatened species richness map to the range of 0–100 (%) using the minimum-maximum normalisation method, with 100% having the highest threatened species richness and 0% having the lowest threatened species richness. We defined AHRTMS as those containing the top 20% of the cumulated area of threatened species richness¹⁰⁷. By this definition, there was a total about 8,105,865.9 km² of global mountains contained within AHRTMS (Supplementary Fig. 4b).

We distinguished PAs, AHRTMS-inside PAs and AHRTMS-outside PAs (Fig. 3a). Next, we used spatial overlay analysis of these three layers together with the layer of MVL loss to evaluate the spatial coincidence between MVL loss within PAs, AHRTMS-inside PAs and AHRTMS-outside PAs, including the magnitudes of loss, as well as its drivers (Fig. 3b, Supplementary Fig. 5 and Supplementary Table 4).

Accuracy evaluation and analysis

We adopted two strategies to assess the reliability of our findings. Firstly, although the impervious surface we used is defined as an artificial impervious surface and was used as a proxy for human settlement growth, there may be natural bare rock and soil that were mistakenly classified as artificial surfaces. To incorporate this, we randomly selected a total 5209 samples from impervious surfaces in 2000 and 2020 using a random function to assess the ratio of artificial and natural surfaces (i.e., natural bare rock/soil) in impervious surfaces. Secondly, in order to thoroughly verify the accuracy of our estimates of global MVL loss, we randomly selected a total 16,478 samples using a random function from global mountain areas. These stratified random samples were uniformly and randomly distributed across areas where MVL losses were due to human expansion (4138 samples) and natural disasters (3704 samples), and areas without MVL loss (including nonvegetated mountain areas) (8636 samples) (Supplementary Fig. 10). By selecting samples in non-MVL loss areas, we can ensure that there was no significant omission of MVL loss, and simultaneously assess potential land cover misclassifications.

All samples were tagged geographically with Keyhole Markup Language and placed into Google Earth Pro. We used all cloudless historical high-solution images (e.g., EarlyBird-1 (0.8–3.0 m), IKONOS (3.2 m), QuickBird (0.6–2.4 m), GeoEye-1 (0.41–1.65 m), WorldView (0.25–1.84 m), Pleiades-1A (0.5–2.0 m), Pleiades-1B (0.5–2.0 m), SPOT-6 and SPOT-7 (1.5–6.0 m), RapidEye (5 m), Doves (3 m) etc.) stored in Google Earth Pro to assess the result reliability. When high-resolution images were lacking at the sample points, we used ESA Sentinel-2 (10 m) and Landsat TM/ETM+/OLI (30 m) imageries to determine result reliability.

To assess the reliability of impervious surface (year of 2000 and 2020) and the ratio of artificial and natural surface in impervious surface, we labelled samples as correct if they were impervious surface in high-resolution satellite imagery; otherwise, they were labelled as incorrect if they were other land types (Supplementary Data 1). After excluding uncertain samples (only accounting for 2.0% of total samples), we found that the accuracy (correct samples/ (total samples-uncertain samples)) of impervious surfaces reaches about 92.4%, with the vast majority being artificial surfaces (85.9%), while the proportion of natural surface-bare rock/soil is relatively small, indicating that impervious surfaces are reliable as a proxy of human settlement growth.

To assess the reliability of human expansion-driven MVL loss (e.g., human settlement growth, agriculture expansion and mining), we labelled samples as correct if they were MVL surfaces in 2000 (e.g., forest, shrubland or grassland), but not in 2020 (i.e., converted to impervious surface, cropland or mining surface); otherwise, they were labelled as incorrect (Supplementary Data 2). To assess the reliability of natural disaster-driven MVL loss (e.g., wildfires, floods, landslides and droughts), we labelled samples as correct if they were MVL

surfaces in 2000, but not in 2020 (i.e., converted to non-artificial surfaces without vegetation or near non-vegetation); otherwise, they were labelled as incorrect (Supplementary Data 3). To assess the reliability of non-MVL loss, we labelled non-MVL loss samples as correct if they were non-MVL surfaces in 2000 and non-MVL surfaces/MVL surfaces in 2020, or if they were MVL surfaces in both 2000 and 2020; otherwise, they were labelled as incorrect results (Supplementary Data 4).

We used a team with specialised knowledge and training in standard procedures and risk assessment to interpret all the above samples. When samples could not be determined during visual interpretation, these samples were labelled as uncertain.

After excluding uncertain samples (only accounting for 1.4 % of total samples), we calculated the overall accuracy (OA = correct samples/ (total random samples-uncertain samples)) of global mapping, as well as the producer's accuracy (PA = correct samples of MVL loss/ (correct samples of MVL loss + incorrect samples of non-MVL loss)) and user's accuracy (UA = correct samples of MVL loss/ (total random samples of MVL loss-uncertain samples)) of MVL loss¹⁰⁸. We estimated these accuracies at different scales, including global scale, continent scale (i.e., separate ten world regions) and biodiversity hotspot scale (i.e., PAs and AHRTMS outside of PAs). We found that the overall accuracy of global mapping was 88.2% (Supplementary Table 1), and the producer's accuracy and user's accuracy of MVL loss, respectively, reached 90.7% and 84.0% (Supplementary Table 1).

Uncertainties and limitations

Despite our comprehensive assessment of global MVL loss, there are uncertainties and limitations that need to be clarified and further explored. The large-scale earth observation data at 30-m resolution is relatively high for global assessments, but it may still overlook fine-scale changes in complex mountain terrains, potentially leading to slight under- or overestimation of MVL loss in certain regions. Future studies could employ higher-resolution datasets to enhance spatial accuracy. Although our defined AHRTMS represent the areas of the high richness of threatened mountain-occurring species, we recognise it uses relatively coarse range maps to draw conclusions about biodiversity in complex mountain landscapes that may bring uncertainties. Our classification of MVL loss drivers is based on final land cover transitions, which may overlook specific land cover processes underlying the loss. Future work could refine this framework by distinguishing key subtypes (e.g., subdividing agriculture expansion into commodity-driven agriculture, horticulture and orchards, and plantations and subdividing human settlement growth into urban sprawl and tourism development) to better capture the diversity and ecological impacts of MVL loss drivers. We also acknowledge that our study focuses solely on MVL loss driven by human expansions and natural disasters, and neglects potential MVL gains in other areas (e.g., the transition from human-used land to vegetated landscapes). Future work should consider these gains to comprehensively understand the dynamic processes of vegetated landscapes. Furthermore, there are some drivers of MVL loss that are not fully captured by our analyses, such as insect outbreaks or diseases. Future work will be needed to explore more particular drivers. In addition, we did not capture seasonal variability of grasslands, which may create uncertainties and limitations in structurally unstable regions (e.g., climate transition zones or complex landscapes). Future work should incorporate seasonal grassland dynamics to enhance ecological validity and temporal sensitivity. Meanwhile, we did not distinguish between canyons and typical mountains. Addressing this distinction at higher resolutions or regional scales could offer new insights into the roles played by heterogeneous mountain geomorphic units in landscape and biodiversity dynamics.

Reporting summary

Further information on research design is available in the Nature Portfolio Reporting Summary linked to this article.

Data availability

Global mountain boundaries can be downloaded from the GMBA (https://www.earthenv.org/mountains). Global land cover datasets (GLC FCS30D) are freely available from Zenodo (https://doi.org/10. 5281/zenodo.8239305). Two global mining distribution datasets are available for download from PANGAEA (10.1594/PANGAEA.942325) and Zenodo (https://zenodo.org/records/7894216). Landslide data can be obtained from NASA-GLC (https://catalog.data.gov/dataset/globallandslide-catalog-export). Global annual burned area maps can be downloaded from Harvard Dataverse (https://doi.org/10.7910/DVN/ 3CTMKP). Global flood data can be collected from GFD at http://globalflood-database.cloudtostreet.info/. Global TVDI data can be obtained from the National Earth System Science Data Centre of China (http:// www.geodata.cn/). Global Landsat images (TM/ETM+/OLI) can be collected from USGS. Global threatened species (mammals, amphibians, reptiles and plants) can be obtained from the IUCN Red List database (https://www.iucnredlist.org), while threatened bird species can be obtained from the Birdlife International website (http:// datazone.birdlife.org/home). Global PAs are freely available from WDPA (https://www.protectedplanet.net/en). The validation dataset of MVL loss is available in the supplementary documents (Supplementary Data 2-4). The global MVL loss map, mountain PAs and AHRTMS are shared in the Zenodo repository: (https://zenodo.org/records/ 15767019).

Code availability

No special code was used. All map-related operations were performed using the ArcGlS (10.8) platform (www.esri.com/en-us/arcgis); global annual composite NDVI was produced in Google Earth Engine (https://code.earthengine.google.com/25f74defdace54434a5edfaf6c9eba42). Analyses can be reproduced following the procedures described in the Methods.

References

- Rahbek, C. et al. Humboldt's enigma: What causes global patterns of mountain biodiversity?. Science 365, 1108–1113 (2019).
- Rahbek, C. et al. Building mountain biodiversity: Geological and evolutionary processes. Science 365, 1114–1119 (2019).
- 3. Perrigo, A., Hoorn, C. & Antonelli, A. Why mountains matter for biodiversity. *J. Biogeogr.* **47**, 315–325 (2020).
- 4. Mitchard, E. T. A. The tropical forest carbon cycle and climate change. *Nature* **559**, 527–534 (2018).
- Peters, M. K. et al. Climate-land-use interactions shape tropical mountain biodiversity and ecosystem functions. *Nature* 568, 88–92 (2019).
- Price, M. F., Butt, N. Forests in Sustainable Mountain Development: a State of Knowledge Report for 2000. (CAB International Wallingford, 2000).
- Bengtsson, J. et al. Grasslands-more important for ecosystem services than you might think. Ecosphere 10, 1–20 (2019).
- 8. Ward, A., Dargusch, P., Thomas, S., Liu, Y. & Fulton, E. A. A global estimate of carbon stored in the world's mountain grasslands and shrublands, and the implications for climate policy. *Glob. Environ. Change* **28**, 14–24 (2014).
- UNEP-WCMC. Mountain Watch: Environmental Change and Sustainable Development in Mountains. (Cambridge UK, 2002).
- Ma, S., Qiao, Y. P., Wang, L. J. & Zhang, J. C. Terrain gradient variations in ecosystem services of different vegetation types in mountainous regions: Vegetation resource conservation and sustainable development. *Ecol. Manag.* 482, 118856 (2021).
- Reid, W. V. et al. Ecosystems and Human Well-being-Synthesis: A Report of the Millennium Ecosystem Assessment. (Island Press. 2005).
- 12. UN. Sustainable Development: Target no.1 of SDG 15. Available at https://sdgs.un.org/topics/mountains (2023).

- Schickhoff, U., Bobrowski, M., Mal, S., Schwab, N., Singh, R. Sustainable Development Goals Series. (Springer Cham, 2022).
- Chakraborty, A. Mountains as vulnerable places: a global synthesis of changing mountain systems in the Anthropocene. Geojournal 86, 585–604 (2021).
- Yang, C. et al. Characteristics and trends of hillside urbanization in China from 2007 to 2017. Habitat Int. 120, 102502 (2022).
- Yang, C. et al. Human expansion into Asian highlands in the 21st Century and its effects. Nat. Commun. 13, 4955 (2022).
- 17. Shi, K., Cui, Y., Liu, S. & Wu, Y. Global urban land expansion tends to be slope climbing: a remotely sensed nighttime light approach. *Earths Future* **11**, 1–14 (2023).
- Li, P., Qian, H. & Wu, J. Environment: Accelerate research on land creation. *Nature* 510, 29–31 (2014).
- Feng, Y. et al. Upward expansion and acceleration of forest clearance in the mountains of Southeast Asia. *Nat. Sustain.* 4, 892–899 (2021).
- Zeng, Z. Z. et al. Highland cropland expansion and forest loss in Southeast Asia in the twenty-first century. *Nat. Geosci.* 11, 556–562 (2018).
- 21. Potapov, P. et al. Global maps of cropland extent and change show accelerated cropland expansion in the twenty-first century. *Nat. Food* **3**, 19–28 (2022).
- 22. Maus, V. et al. An update on global mining land use. Sci. Data 9, 1–11 (2022)
- Tang, L. & Werner, T. T. Global mining footprint mapped from high-resolution satellite imagery. Comm. Earth Environ. 4, 163 (2023).
- 24. DeFries, R. S., Rudel, T., Uriarte, M. & Hansen, M. Deforestation driven by urban population growth and agricultural trade in the twenty-first century. *Nat. Geosci.* **3**, 178–181 (2010).
- Curtis, P. G., Slay, C. M., Harris, N. L., Tyukavina, A. & Hansen, M. C. Classifying drivers of global forest loss. Science 361, 1108–1111 (2018).
- Gonzalez-Gonzalez, A., Clerici, N. & Quesada, B. Growing mining contribution to Colombian deforestation. *Environ. Res. Lett.* 16, 064046 (2021).
- Coronese, M., Lamperti, F., Keller, K., Chiaromonte, F. & Roventini, A. Evidence for sharp increase in the economic damages of extreme natural disasters. *Proc. Natl. Acad. Sci. USA* 116, 21450–21455 (2019).
- Otto, F. E. L. et al. Attributing high-impact extreme events across timescales-a case study of four different types of events. *Clim. Change* 149, 399–412 (2018).
- Aalst, M. K. V. The impacts of climate change on the risk of natural disasters. Disasters 30, 5–18 (2006).
- Coop, J. D. et al. Wildfire-driven forest conversion in western north american landscapes. *Bioscience* 70, 659–673 (2020).
- 31. Pausas, J. G. & Keeley, J. E. Wildfires and global change. Front. Eco. Environ. 19, 387–395 (2021).
- Stone, R. Landslides, flooding pose threats as experts survey Quake's impact. Science 320, 996–997 (2008).
- Korup, O., Seidemann, J. & Mohr, C. H. Increased landslide activity on forested hillslopes following two recent volcanic eruptions in Chile. Nat. Geosci. 12, 284–289 (2019).
- Xu, C. et al. Increasing impacts of extreme droughts on vegetation productivity under climate change. *Nat. Clim. Change* 9, 948–953 (2019).
- Bousfield, C. G., Lindenmayer, D. B. & Edwards, D. P. Substantial and increasing global losses of timber-producing forest due to wildfires. *Nat. Geosci.* 16, 1145–1150 (2023).
- 36. Bowman, D. M. J. S. et al. Vegetation fires in the Anthropocene. Nat. Rev. Earth Environ. 1, 500–515 (2020).
- Convention on Biological Diversity. Kunming-Montreal Global Biodiversity Framework. (CBD, 2022).

- Ceccherini, G. et al. Abrupt increase in harvested forest area over Europe after 2015. Nature 583, 72–77 (2020).
- van Vliet, J. Direct and indirect loss of natural area from urban expansion. Nat. Sustain 2, 755–763 (2019).
- UN. Kunming Declaration. Declaration from the High-Level Segment of the UN Biodiversity Conference 2020 (Part 1) Under the Theme: "Ecological Civilization: Building a Shared Future for All Life on Earth" (Final Draft) (United Nations Biodiversity Conference, 2021).
- 41. Brodie, J. F. et al. Landscape-scale benefits of protected areas for tropical biodiversity. *Nature* **620**, 807–812 (2023).
- Peng, L., Searchinger, T. D., Zionts, J. & Waite, R. The carbon costs of global wood harvests. *Nature* 620, 110–115 (2023).
- 43. Schug, F. et al. The global wildland-urban interface. *Nature* **621**, 94–99 (2023).
- Bar-Massada, A., Radeloff, V. C. & Stewart, S. I. Biotic and abiotic effects of human settlement in the wildland-urban interface. Bioscience 64, 429–437 (2014).
- Chen, B. et al. Wildfire risk for global wildland-urban interface areas. Nat. Sustain. 7, 474-484 (2024).
- Dai, Y. et al. Conflicts of human with the Tibetan brown bear (Ursus arctos pruinosus) in the Sanjiangyuan region, China. Glob. Eco. Conser. 22, e01039 (2020).
- Soulsbury, C. D. & White, P. C. L. Human-wildlife interactions in urban areas: a review of conflicts, benefits and opportunities. Wildl. Res. 42, 541–553 (2015).
- 48. Yin, D., Yuan, Z., Li, J. & Zhu, H. Mitigate human-wildlife conflict in China. Science **373**, 500 (2021).
- Qomariah, I. N., Rahmi, T., Said, Z. & Wijaya, A. Conflict between human and wild Sumatran Elephant (Elephas maximus sumatranus Temminck, 1847) in Aceh Province, Indonesia. *Biodiversitas* 20, 77–84 (2019).
- Aska, B., Franks, D. M., Stringer, M. & Sonter, L. J. Biodiversity conservation threatened by global mining wastes. *Nat. Sustain.* 7, 23–30 (2023).
- Durán, A. P., Rauch, J. & Gaston, K. J. Global spatial coincidence between protected areas and metal mining activities. *Biol. Con*serv. 160, 272–278 (2013).
- Viviroli, D., Kummu, M., Meybeck, M., Kallio, M. & Wada, Y. Increasing dependence of lowland populations on mountain water resources. *Nat. Sustain.* 3, 917–928 (2020).
- 53. Macklin, M. G. et al. Impacts of metal mining on river systems: a global assessment. *Science* **381**, 1345–1350 (2023).
- 54. Hudson-Edwards, K. A. et al. Tailings storage facilities, failures and disaster risk. *Nat. Rev. Earth Environ*. (2024).
- Gebrechorkos, S. H. et al. Warming accelerates global drought severity. *Nature* 642, 628–635 (2025).
- Joao, T., Joao, G., Bruno, M. & Joao, H. Indicator-based assessment of post-fire recovery dynamics using satellite NDVI time-series. *Ecol. Indic.* 89, 199–212 (2018).
- Castillo, S. et al. A recent review of fire behavior and fire effects on native vegetation in Central Chile. Glob. Eco. Conser. 24, e01210 (2020).
- Mi, J. et al. Vegetation patterns on a landslide after five years of natural restoration in the Loess Plateau mining area in China. Ecol. Eng. 136, 46–54 (2019).
- Chen, C. et al. China and India lead in greening of the world through land-use management. *Nat. Sustain.* 2, 122–129 (2019).
- Chazdon, R. L. Beyond deforestation: Restoring forests and ecosystem services on degraded lands. Science 320, 1458–1460 (2008).
- Xu, X. & Zhang, D. Comparing the long-term effects of artificial and natural vegetation restoration strategies: A case-study of Wuqi and its adjacent counties in northern China. *Land Degrad. Dev.* 32, 3930–3945 (2021).

- Tomas, W. M. et al. Distance sampling surveys reveal 17 million vertebrates directly killed by the 2020's wildfires in the Pantanal. Braz. Sci. Rep. 11, 23547 (2021).
- UNEP. Spreading like wildfire: the rising threat of extraordinary landscape fires. https://www.unep.org/resources/report/ spreading-wildfire-rising-threat-extraordinary-landscapefires (2022).
- Li, B. V., Jenkins, C. N. & Xu, W. Strategic protection of landslide vulnerable mountains for biodiversity conservation under landcover and climate change impacts. *Proc. Natl. Acad. Sci. USA* 119, e2113416118 (2022).
- Ward, M. et al. Impact of 2019–2020 mega-fires on Australian fauna habitat. *Nat. Eco. Evol.* 4, 1321–1326 (2020).
- Barlow, J. et al. Anthropogenic disturbance in tropical forests can double biodiversity loss from deforestation. *Nature* 535, 144–147 (2016).
- Betts, M. G. et al. Global forest loss disproportionately erodes biodiversity in intact landscapes. Nature 547, 441–444 (2017).
- Phalan, B., Onial, M., Balmford, A. & Green, R. E. Reconciling food production and biodiversity conservation: land sharing and land sparing compared. Science 333, 1289–1291 (2011).
- 69. Brennan, A. et al. Functional connectivity of the world's protected areas. Science **376**, 1101–1104 (2022).
- Laurance, W. F., Sayer, J. & Cassman, K. G. Agricultural expansion and its impacts on tropical nature. *Trends Ecol. Evol.* 29, 107–116 (2014).
- Ren, Q. et al. Impacts of urban expansion on natural habitats in global drylands. Nat. Sustain. 5, 869–878 (2022).
- 72. Kong, L. Q. et al. Natural capital investments in China undermined by reclamation for cropland. *Nat. Ecol. Evol.* **7**, 1771–1777 (2023).
- Hansen, M. C. et al. The fate of tropical forest fragments. Sci. Adv.
 6, 8574 (2020).
- Sharkey, W., Milner-Gulland, E. J., Sinovas, P. & Keane, A. A framework for understanding the contributions of local residents to protected area law enforcement. *Oryx* 58, 746–758 (2024).
- Chen, X. et al. Establishing a protected area network in Xinlong with other effective area-based conservation measures. Conserv. Biol. 38, e14297 (2024).
- Bateman, I. & Balmford, A. Current conservation policies risk accelerating biodiversity loss. Nature 618, 671–674 (2023).
- 77. IPCC. Climate Change 2013. (Cambridge Univ. Press, 2013).
- 78. Grekousis, G., Mountrakis, G. & Kavouras, M. An overview of 21 global and 43 regional land-cover mapping products. *Int. J. Remote Sens.* **36**, 5309–5335 (2015).
- 79. Buchhorn, M. et al. Copernicus global land cover layers-collection 2. *Remote Sens.* **12**, 1044 (2020).
- 80. Zhang, X. et al. GLC_FCS30: global land-cover product with fine classification system at 30m using time-series Landsat imagery. *Earth Syst. Sci. Data* **13**, 2753–2776 (2021).
- 81. ESA. ESA's WorldCover. https://esa-worldcover.org/en/data-access (2024).
- 82. Liu, L. et al. Finer-resolution mapping of global land cover: recent developments, donsistency analysis, and prospects. *J. Remote Sens.* **2021**, 5289697 (2021).
- 83. Zhang, X. et al. GLC_FCS30D: the first global 30 m land-cover dynamics monitoring product with a fine classification system for the period from 1985 to 2022 generated using dense-time-series Landsat imagery and the continuous change-detection method. Earth Syst. Sci. Data 16, 1353–1381 (2024).
- Liu, L. Y. & Zhang, X. Algorithm, Progresses, Datasets and Validation of GLC_FCS30D: the first global 30 m land-cover dynamic product with fine classification system from 1985 to 2022. ISPRS Ann. Photogramm. Remote Sens. Spat. Inf. Sci. X-2-2024, 137–143 (2024).

- 85. Amantai, N., Meng, Y. Y., Wang, J. Z., Ge, X. Y. & Tang, Z. Y. Climate overtakes vegetation greening in regulating spatiotemporal patterns of soil moisture in arid Central Asia in recent 35 years. *GISci. Remote Sens.* **61**, 2286744 (2024).
- 86. UNEP-WCMC. Mountains of the World-2002. (Cambridge UK, 2002).
- 87. Snethlage, M. A. et al. GMBA Mountain Inventory v2. (2022).
- 88. Snethlage, M. A. et al. A hierarchical inventory of the world's mountains for global comparative mountain science. *Sci. Data* **9**, 149 (2022).
- 89. Hock, R. et al. High Mountain Areas. In: IPCC Special Report on the Ocean and Cryosphere in a Changing Climate.(IPCC, 2019).
- Helbig, M. et al. Regional atmospheric cooling and wetting effect of permafrost thaw-induced boreal forest loss. *Glob. Change Biol.* 22, 4048–4066 (2016).
- Bian, J. H. et al. Global high-resolution mountain green cover index mapping based on Landsat images and Google Earth Engine. ISPRS J. Photogramm. Remote Sens. 162, 63–76 (2020).
- 92. Gong, P., Li, X. & Zhang, W. 40-Year (1978-2017) human settlement changes in China reflected by impervious surfaces from satellite remote sensing. Sci. Bull. **64**, 756-763 (2019).
- 93. Zhang, X. X. et al. A large but transient carbon sink from urbanization and rural depopulation in China. *Nat. Sustain.* **5**, 321–328 (2022).
- Long, T. et al. 30 m resolution global annual burned area mapping based on Landsat images and Google Earth Engine. *Remote Sens.* 11, 489 (2019).
- 95. Tellman, B. et al. Satellite imaging reveals increased proportion of population exposed to floods. *Nature* **596**, 80–86 (2021).
- Kirschbaum, D. B., Adler, R., Hong, Y., Hill, S. & Lerner-Lam, A. A global landslide catalog for hazard applications: method, results, and limitations. *Natl Hazards* 52, 561–575 (2010).
- Kirschbaum, D., Stanley, T. & Zhou, Y. P. Spatial and temporal analysis of a global landslide catalog. *Geomorphology* 249, 4–15 (2015).
- 98. National Earth System Science Data Center. Global 1km resolution TVDI dataset. Available at: http://www.geodata.cn (2023).
- Liu, L. et al. The Microwave Temperature Vegetation Drought Index (MTVDI) based on AMSR-E brightness temperatures for long-term drought assessment across China (2003-2010). Remote Sens. Environ. 199, 302–320 (2017).
- 100. Choat, B. et al. Triggers of tree mortality under drought. *Nature* **558**, 531–539 (2018).
- Tucker, C. J. Red and photographic infrared linear combinations for monitoring vegetation. *Remote Sens. Environ.* 8, 127–150 (1979).
- 102. Huang, S., Tang, L., Hupy, J. P., Wang, Y. & Shao, G. A commentary review on the use of normalized difference vegetation index (NDVI) in the era of popular remote sensing. *J. Forestry Res.* 32, 1–6 (2021).
- Roy, D. P. et al. Characterization of Landsat-7 to Landsat-8 reflective wavelength and normalized difference vegetation index continuity. *Remote Sens. Environ.* 185, 57–70 (2016).
- 104. Yan, J., Zhang, G., Ling, H. & Han, F. Comparison of time-integrated NDVI and annual maximum NDVI for assessing grassland dynamics. Ecol. Indic. 136, 108611 (2022).
- Li, L. et al. Increasing sensitivity of alpine grasslands to climate variability along an elevational gradient on the Qinghai-Tibet Plateau. Sci. Total Environ. 678, 21–29 (2019).
- IUCN. A Global Standard for the Identification of Key Biodiversity Areas Version 1.0 (IUCN, 2016).
- Xu, W. et al. Strengthening protected areas for biodiversity and ecosystem services in China. Proc. Natl. Acad. Sci. USA 114, 1601–1606 (2017).

 Olofsson, P. et al. Good practices for estimating area and assessing accuracy of land change. Remote Sens. Environ. 148, 42–57 (2014).

Acknowledgements

We thank many students and colleagues for their careful validation work. We also thank all the institutions and platforms for providing support, including GMBA, WDPA, IUCN, National Earth System Science Data Centre of China, USGS, ESA, NASA and Google Earth Engine. This study was supported by the National Natural Science Foundation of China (No. 42471312, 42201319, 42371337 and 42301454) and the discipline breakthrough pioneer project of the Ministry of Education of the People's Republic of China.

Author contributions

C.Y. and Q.L. designed the study; C.Y., H.X., X.W. and J.C. conducted data analyses; C.Y. and H.X. prepared the manuscript; J.M.C. reviewed and edited the manuscript; C.Y., B.T., W.T., Y.Z., T.S., M.C., W.M., H.L. and many students conducted sample validation work; All authors contributed to the results.

Competing interests

The authors declare no competing interests.

Additional information

Supplementary information The online version contains supplementary material available at https://doi.org/10.1038/s41467-025-64449-0.

Correspondence and requests for materials should be addressed to Qingquan Li.

Peer review information *Nature Communications* thanks Paul Ramsay and the other anonymous reviewer(s) for their contribution to the peer review of this work. A peer review file is available.

Reprints and permissions information is available at http://www.nature.com/reprints

Publisher's note Springer Nature remains neutral with regard to jurisdictional claims in published maps and institutional affiliations.

Open Access This article is licensed under a Creative Commons Attribution-NonCommercial-NoDerivatives 4.0 International License, which permits any non-commercial use, sharing, distribution and reproduction in any medium or format, as long as you give appropriate credit to the original author(s) and the source, provide a link to the Creative Commons licence, and indicate if you modified the licensed material. You do not have permission under this licence to share adapted material derived from this article or parts of it. The images or other third party material in this article are included in the article's Creative Commons licence, unless indicated otherwise in a credit line to the material. If material is not included in the article's Creative Commons licence and your intended use is not permitted by statutory regulation or exceeds the permitted use, you will need to obtain permission directly from the copyright holder. To view a copy of this licence, visit https://creativecommons.org/licenses/by-nc-nd/4.0/.

© The Author(s) 2025